

# SyncHuman: Synchronizing 2D and 3D Generative Models for Single-view Human Reconstruction

Wenyue Chen<sup>1</sup>, Peng Li<sup>2†</sup>, Wangguandong Zheng<sup>3</sup>, Chengfeng Zhao<sup>2</sup>  
Mengfei Li<sup>2</sup>, Yaolong Zhu<sup>1</sup>, Zhiyang Dou<sup>4</sup>, Ronggang Wang<sup>1</sup>, Yuan Liu<sup>2†</sup>

<sup>1</sup>PKU, <sup>2</sup>HKUST, <sup>3</sup>SEU, <sup>4</sup>MIT

<https://xishuxishu.github.io/SyncHuman.github.io>



Figure 1: We introduce **SyncHuman**, a full-body human reconstruction model using synchronized 2D and 3D diffusion model. Given a single image of a clothed person, our method generates detailed geometry and lifelike 3D human appearances across diverse poses.

## Abstract

Photorealistic 3D full-body human reconstruction from a single image is a critical yet challenging task for applications in films and video games due to inherent ambiguities and severe self-occlusions. While recent approaches leverage SMPL estimation and SMPL-conditioned image generative models to hallucinate novel views, they suffer from inaccurate 3D priors estimated from SMPL meshes and have difficulty in handling difficult human poses and reconstructing fine details. In this paper, we propose SyncHuman, a novel framework that combines 2D multiview generative model and 3D native generative model for the first time, enabling high-quality clothed human mesh reconstruction from single-view images even under challenging human poses. Multiview generative model excels at capturing fine 2D details but struggles with structural consistency, whereas 3D native generative model generates coarse yet structurally consistent 3D shapes. By

<sup>†</sup>Corresponding authors

integrating the complementary strengths of these two approaches, we develop a more effective generation framework. Specifically, we first jointly fine-tune the multiview generative model and the 3D native generative model with proposed pixel-aligned 2D-3D synchronization attention to produce geometrically aligned 3D shapes and 2D multiview images. To further improve details, we introduce a feature injection mechanism that lifts fine details from 2D multiview images onto the aligned 3D shapes, enabling accurate and high-fidelity reconstruction. Extensive experiments demonstrate that SyncHuman achieves robust and photo-realistic 3D human reconstruction, even for images with challenging poses. Our method outperforms baseline methods in geometric accuracy and visual fidelity, demonstrating a promising direction for future 3D generation models.

## 1 Introduction

Reconstructing 3D clothed humans from a single RGB image is a fundamental yet challenging task. It has broad applications in AR/VR, virtual try-on, gaming, and film production [33, 36]. Compared to parametric body reconstruction [54], clothed human reconstruction [83] requires capturing not only the underlying body shape but also the diverse topology, geometry, and dynamics of garments.

Recent progress in implicit representations and generative models has led to significant advances in this area. PIFu [45] pioneered this direction with predicted neural implicit field, followed by methods such as ICON [63], ECON [62], and PaMIR [82], which introduced improvements in SMPL priors, normal estimation, and feature representation, respectively. With the advancement of generative models techniques [30, 31, 24], recent works [13, 78, 25] have introduced multiview generative model for novel-view human image prediction, enhancing 3D reconstruction fidelity, detail preservation, and robustness.

However, accurately reconstructing 3D clothed humans from a single 2D image is still challenging, especially for images with challenging poses. The reason is that most methods [13, 25] strongly rely on human shape priors, i.e., SMPL estimation, to provide structural information to generate multiview images. Unfortunately, existing single-view human pose estimation methods [7, 72, 1, 39, 3] often lack sufficient accuracy, especially when dealing with occlusions or challenging poses, as shown in Fig. 2 (a). Moreover, the estimated SMPL meshes represent only naked human bodies and fail to accurately model loose clothing. Thus, conditioned on inaccurate SMPL meshes, the multiview generative models often generate images with incorrect body topologies and mismatched details, leading to reconstruction artifacts, as shown in Fig. 2 (b).

An alternative approach employs native 3D generative models [73, 61, 27, 79] to generate the 3D human shapes directly. However, these methods often produce results lacking in detail and fidelity. By training on large-scale 3D datasets, recent 3D native generation methods [61, 79, 27] demonstrate improved capability for constructing 3D human meshes from single-view images, even for challenging human poses, as shown in Fig. 2 (c). However, these 3D native generation methods typically generate only coarse, low-fidelity shapes that poorly match the input image characteristics. Enhancing both the geometric detail and input-consistency of 3D-native generation outputs remains an open challenge.

In this paper, we propose **SyncHuman**, a novel framework that combines 2D multiview generative model and native 3D generative model for the first time, leveraging their complementary strengths to address these challenges, as shown in Fig. 2 (d). Instead of simply relying on the SMPL estimation, we utilize the more accurate

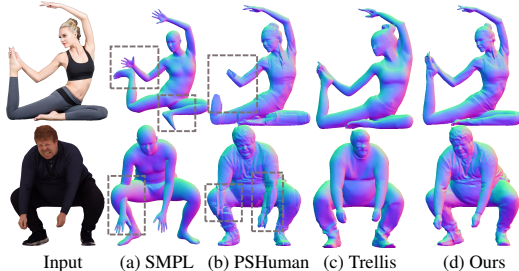


Figure 2: Geometric comparison between SMPL estimation [39], 2D multiview generative model (MVD) PSHuman [25], native 3D generative model Trellis [61] and our method. 2D MVD produces high-quality details but has geometry artifacts when conditioned on inaccurate SMPL meshes. Native 3D generative model produces correct coarse structure but loses fine details and fidelity. Our method combines the strengths of both 2D and 3D generative models to produce detailed 3D human meshes with high fidelity.

3D shapes generated by the native 3D generative model to guide the generation of 2D multiview images, greatly improving the multiview consistency. At the same time, the detailed multiview images also guide the 3D generative model to carve the 3D shapes with detail and high fidelity.

In implementation, SyncHuman consists of two main components. First, we design a unified 2D-3D cross-space generative model with two branches, i.e., a 2D multiview generation branch and a 3D sparse structure generation branch, which interact via 2D-3D synchronization attention layers. The 2D-3D attention layers align the multiview images with the generated 3D shapes, which simultaneously utilize the 3D shapes to improve the cross-view consistency and employ the multiview images to enhance the fidelity of the generated 3D shapes. Next, to obtain high-quality 3D meshes, we design a multiview guided decoder to incorporate the pixel-aligned information of generated multiview images into the 3D generation during the decoding process, which not only carves fine geometric detail but also greatly improves the texture fidelity.

We conduct extensive experiments on multiple datasets to evaluate the effectiveness of SyncHuman. The results demonstrate that the proposed method outperforms previous single-view human reconstruction methods [62, 13, 25] while even achieving higher fidelity and texture quality than the large-scale 3D generative models [61] trained with datasets hundreds of times larger than ours. SyncHuman unifies 2D multiview generative model and native 3D generative model within a unified framework, enabling higher-quality image-to-3D generation with improved fidelity. This demonstrates significant potential for future 3D generation model development.

## 2 Related works

**Single image human reconstruction.** Prior to the advent of generative approaches, single-image human reconstruction primarily followed either explicit or implicit representation paradigms. Explicit methods, including voxel-based techniques [55, 83], visual hull approaches [34], and depth/normal [8, 50, 10] prediction frameworks, offer computational efficiency but often sacrifice local geometric details. The explicit normal integration in ECON [62] made a significant advancement in reconstruction robustness for the explicit paradigm. In contrast, implicit methods emerged as the dominant approach due to their continuous representation capabilities. The field was revolutionized by PIFu [45, 6, 67], which established pixel-aligned implicit functions for detailed geometry recovery from single images. Subsequent approaches enhance the robustness [11, 63, 82, 68] through parametric body model integration and additional supervision from surface normals [46] and depth information [70, 81]. Most recent works [77, 78, 18, 69, 42, 41] incorporate transformer architecture and utilize large-scale human datasets to reduce inductive bias, enhancing the generalization capability. While these methods demonstrate exceptional performance in handling complex clothing and topological variations, they remain inherently constrained by their reliance on the input image, struggling with photorealistic appearance and detail recovery.

**3D Generation.** 3D generation has been significantly advanced by generative models, which can be roughly categorized into multiview generation approaches and native 3D generation methods. Multiview generation techniques [49, 31, 30, 24, 25, 17, 56, 85, 52, 65, 64, 57, 59, 53] typically employ a two-stage pipeline: first generating consistent multiview images, followed by either optimization-based reconstruction [37] or feed-forward generation [22, 23]. The multiview generation stages involve fine-tuning an image generative model [43] or video generative models [2] by incorporating view-aware attention layers to ensure cross-view consistency. Native 3D generative models [80, 61, 27, 79, 5, 71, 60, 26] operate directly in 3D representation spaces (e.g., 3D Volume [61] or Signed Distance Field [38]), typically comprising a large variational autoencoder combined with a latent diffusion transformer (DiT) [40]. Trained on extensive 3D datasets, these models demonstrate exceptional geometric quality and strong generalization capabilities. Building upon these foundations, our work adapts and fine-tunes such a native 3D generator specifically for human body shape while preserving its generalization capacity.

**Generative Human Reconstruction** Generative models, such as Stable Diffusion, have emerged as a powerful tool for 3D human reconstruction. Pioneering works [28, 16, 15] employ score distillation sample (SDS) to optimize textured human mesh per case, which is time-consuming and typically only text-constrained. Feed-forward methods [13, 4] leverage pose-guided ControlNet [74] to predict plausible back views for neural reconstruction or Gaussian splatting, but their robustness suffers from

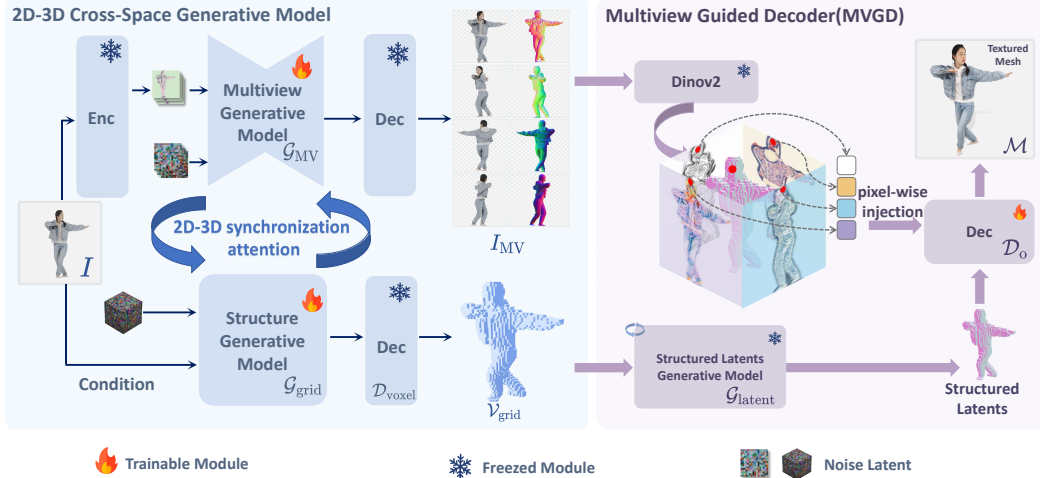


Figure 3: **Overview.** Given a single human image, SyncHuman first generates multiview color and normal maps, along with an aligned sparse voxel grid, which is further transformed into a set of structured latents. Then, we propose to inject the high-quality images into the 3D latents via a Multiview Guided Decoder and output the detailed high-fidelity textured human mesh.

limited multiview cues. Other approaches [20, 25] address this problem by fine-tuning 2D generative models to produce sparse multiview human generations. Despite improved performance, these models struggle with cross-view consistency, leading to inevitable appearance artifacts. Human3Diff [66] attempts to enhance multiview coherence by integrating 3D representations as intermediate constraints during the denoising process. However, reliance on 2D denoising generative models often leads to anatomically implausible human structures due to the absence of body prior. Unlike prior work, this study aims to align the pretrained 2D multiview and 3D native generative models, enabling producing geometrically consistent and robust 3D human models without reliance on any human prior.

### 3 Method

**Overview.** SyncHuman aims to reconstruct a 3D clothed human mesh from a single color image. As shown in Fig. 3, given a full-body human image, we first propose a 2D-3D Cross-Space generative model (Section 3.1) to synthesize multiview color and normal maps, along with an aligned sparse 3D voxel grid, which is further transformed to an aligned structured latent through a pretrained flow transformer. Then, a Multiview Guided Decoder (Section 3.2) is introduced to decode the structured latents into a high-quality, detailed, textured mesh with the help of generated multiview images.

#### 3.1 2D-3D Cross-Space Generative Model

Multiview generative models have shown powerful novel-view generation and generalization capability. Given a human image as input, they could hallucinate multiple views with high-resolution details such as identity, skin texture, and clothing wrinkles, but often struggle with cross-view consistency. In contrast, native 3D generative models naturally maintain 3D structural consistency, yet typically lack fidelity. In this section, we introduce 2D-3D Cross-Space Generative Model, which combines the strengths of 2D multiview generative models and native 3D generative models.

**Multiview Generative Model.** Taking the input image  $I$  as the front view, we use the network structure from PSHuman [25] to generate color and normal maps on four predefined orthogonal viewpoints, front, back, left, and right, which employs an efficient row-wise multiview attention to enhance cross-view consistency. This module could be formulated as

$$I_{MV} = \mathcal{G}_{MV}(I), \quad (1)$$

where  $I_{MV}$  is the generated multiview images and normal maps. Previous methods [25, 78, 13] usually use the estimated 3D SMPL meshes to improve the multiview consistency in  $I_{MV}$ , but often

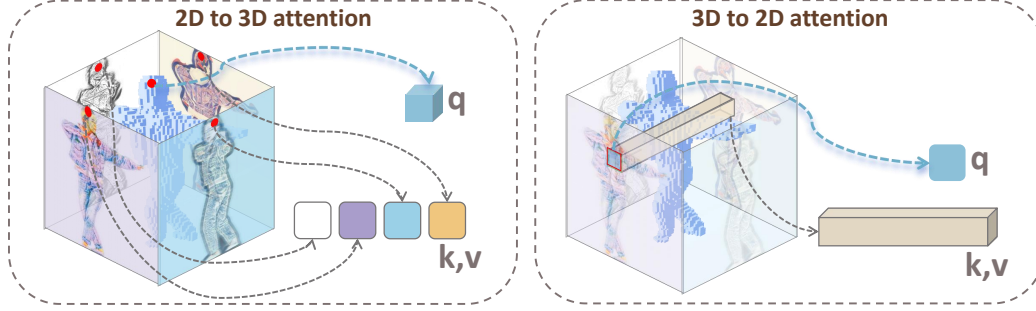


Figure 4: **2D-3D synchronization attention.** **2D to 3D attention:** each 3D voxel feature is orthogonally projected onto front, back, left, and right view planes to retrieve corresponding 2D features, and refines the voxel feature with cross-attention. **3D to 2D attention:** each 2D multiview feature is projected into 3D space to attend to a column of voxel features, enhancing the 2D features. This mutual refinement ensures that 2D generative model and 3D generative model align with each other in a shared 3D space.

suffer from inaccurate SMPL estimation. Thus, we introduce the native 3D generative model to provide 3D structural guidance for the multiview generation in the following.

**3D structure Generative Model.** Our native 3D generative model follows Trellis [61]. A 3D noise grid is first used to produce a sparse structure latent through a DiT-based flow transformer  $\mathcal{G}_{\text{grid}}$ . The sparse structure latent is subsequently decoded into an occupied voxel grid  $\mathcal{V}_{\text{grid}}$  via a Conv-based decoder  $\mathcal{D}_{\text{voxel}}$ ,

$$\mathcal{V}_{\text{grid}} = \mathcal{D}_{\text{voxel}}(\mathcal{G}_{\text{grid}}(I)), \quad (2)$$

where the input image  $I$  is fed into the generative model layer by cross-attention layers. The sparse structure generated by Trellis [61] produces reasonable 3D shapes but loses fidelity and details. We add a novel 2D-3D synchronization attention to improve the fidelity and retrieve more details from multiview images when transforming the 3D structure to textured meshes.

**2D-3D synchronization attention.** We introduce a 2D-3D synchronization attention mechanism between the 2D multiview generative model and the 3D generative model to let them benefit each other in the generation. This consists of 2D to 3D attention and 3D to 2D attention layers as follows.

**(1) 2D to 3D attention.** As shown in Fig. 4, for each 3D voxel feature, we first sample the corresponding 2D features on generated four normal maps. Then, the 3D voxel feature is used as the query token, and the concatenated 2D features from four views serve as keys and values for cross-attention. The cross-attended features are processed by an output MLP with zero initialization, and the resulting features are added to the original 3D voxel feature for refinement.

**(2) 3D to 2D attention.** Then, for each 2D feature on multiview images, we query the corresponding 3D voxel columns as in Fig. 4. Then, the 2D feature is used as the query while the 3D voxel feature serves as keys and values for cross-attention. The cross-attended features are processed by an output layer with zero initialization, and the results are added to the 2D features.

**Discussion.** Our method establishes an explicit correspondence between the 2D and 3D generative models, which benefits each branch. Through this synchronized attention, 3D generative model provides 3D structural guidance for the 2D generative model to improve the multiview consistency while the 2D generative model regularizes the 3D generative model to generate shapes that are more aligned with the input image with better fidelity. This integration enables our model to combine the advantages of both approaches: the 2D generative model provides detailed, high-fidelity results, while the 3D generative model ensures structural integrity and robust handling of complex human poses.

**2D-3D joint training.** We employ the flow matching [29] objective to train our 2D-3D cross-space generative model with the training loss defined by

$$\mathcal{L} = \|\mathbf{v}_{\theta}^{2d}(\mathbf{x}_t^{2d}, I) - (\mathbf{x}_0^{2d} - \epsilon^{2d})\|_2^2 + \|\mathbf{v}_{\theta}^{3d}(\mathbf{x}_t^{3d}, I) - (\mathbf{x}_0^{3d} - \epsilon^{3d})\|_2^2, \quad (3)$$

where  $\epsilon^{2d}$  and  $\epsilon^{3d}$  is the 2D noise maps and 3D noise grid,  $x_t^{2d}$  and  $x_t^{3d}$  is the latent features at timestep  $t$  and  $v_\theta^{2d}$  and  $v_\theta^{3d}$  are the corresponding predicted velocity during denoising process, respectively. Note that the multiview generative model is based on the Stable Diffusion 2.1 [44], and we retarget it to the same flow matching model as Trellis for jointly training.

### 3.2 Multiview Guided Decoder (MVG D)

This section utilizes the generated multiview images and sparse voxels to recover textured 3D meshes.

**Structured latent generation.** We first apply another DiT-based generative model  $\mathcal{G}_{\text{latent}}$  in Trellis [61], which is named as Structured Latents Generative Model in Fig. 3, to generate a set of structured latents  $\mathcal{V}_{\text{latent}}$ . Each of them is attached to a previously generated 3D voxel. These structured latents can be processed by either a mesh decoder  $\mathcal{D}_m$  or a 3D Gaussian Splatting [19] (3DGS) decoder  $\mathcal{D}_{gs}$  to generate a mesh or a 3DGS representation. For simplicity, we unify these decoders as  $\mathcal{D}_o$ . However, directly decoding these latent to mesh or 3DGS leads to a lack of reconstruction details, particularly noticeable in areas such as the face and clothing wrinkles, as demonstrated in Fig. 8. To address this, we propose a multiview feature injection mechanism to incorporate the generated high-resolution multiview images into the original decoder.

**Multiview feature injection.** Specifically, we extract DINOv2 [35] features of generated multiview images, and process them with several trainable MLP layers. For each 3D voxel, we query the corresponding four-view image features and concatenate them with the generated structure latent. The concatenated features are first passed through a MLP, and the resulting representations are subsequently fed into the original decoder  $\mathcal{D}_o$  to produce a high-quality mesh and 3DGS representation. This simple but efficient feature injection allows for preserving the geometry fidelity and appearance realism to a great extent, as shown in Fig. 8. We render images from 3DGS and then bake onto the mesh to obtain the final textured human mesh  $\mathcal{M}$ . The overall decoding process can be formulated as

$$\mathcal{M} = \mathcal{D}_o(\mathcal{G}_{\text{latent}}(I, \mathcal{V}_{\text{grid}}), I_{\text{MV}}). \quad (4)$$

**Training Loss.** We train the multiview guided decoder for the 3DGS branch and the mesh branch separately. For the 3DGS branch, we use L1 loss, Structural Similarity Index (SSIM), Learned Perceptual Image Patch Similarity (LPIPS) loss between renderings and ground-truth images, and a regularization loss to avoid extremely large or small opacity. For the mesh branch, we render the foreground mask, depth maps, and normal maps from the generated 3D meshes. Then, we compute the L1 or Huber loss between the ground truth and the renderings to train the decoder. More architectural design and training details are given in the supplementary material.

## 4 Experiments

### 4.1 Experiment Setup

**Dataset.** Our models are trained on several widely used 3D human scanning datasets, including THuman2.1 [70], CustomHumans [12], THuman3.0 [51], and 2K2K [10]. To construct training images, we render 8 ground-truth images using orthographic cameras with evenly distributed azimuth angles and a fixed  $0^\circ$  elevation with a resolution of  $768 \times 768$ . For quantitative evaluation, we utilize 100 scans from X-Humans [47] and 150 scans from CAPE [32]. X-Humans contains 233 sequences of high-quality textured scans from 20 participants. We randomly selected 5 textured scans from each of the 20 participants in the X-Humans dataset, resulting in 100 test samples. Following ICON’s partitioning criteria, we subdivide CAPE into "CAPE-FP" (50 samples) and "CAPE-NFP" (100 samples) to test the generalization ability in real-world examples. We conduct comparison with the baseline methods on the aforementioned X-Humans subset and CAPE subset, and perform ablation experiments on the same X-Humans subset.

**Metric.** To evaluate reconstruction capability, we employ three primary metrics: 1-directional point-to-surface (**P2S**),  $L_1$  Chamfer Distance (**CD**), and Normal Consistency (**NC**). For geometry evaluation, we align the centers of the reconstructed mesh and the ground truth mesh and then scale them so that the coordinate range of the longest axis is 1. For appearance evaluation, we render front, back, left, and right views and compute **PSNR** [58], structural similarity index (**SSIM**) [75], and perceptual image patch similarity (**LPIPS**) [76].

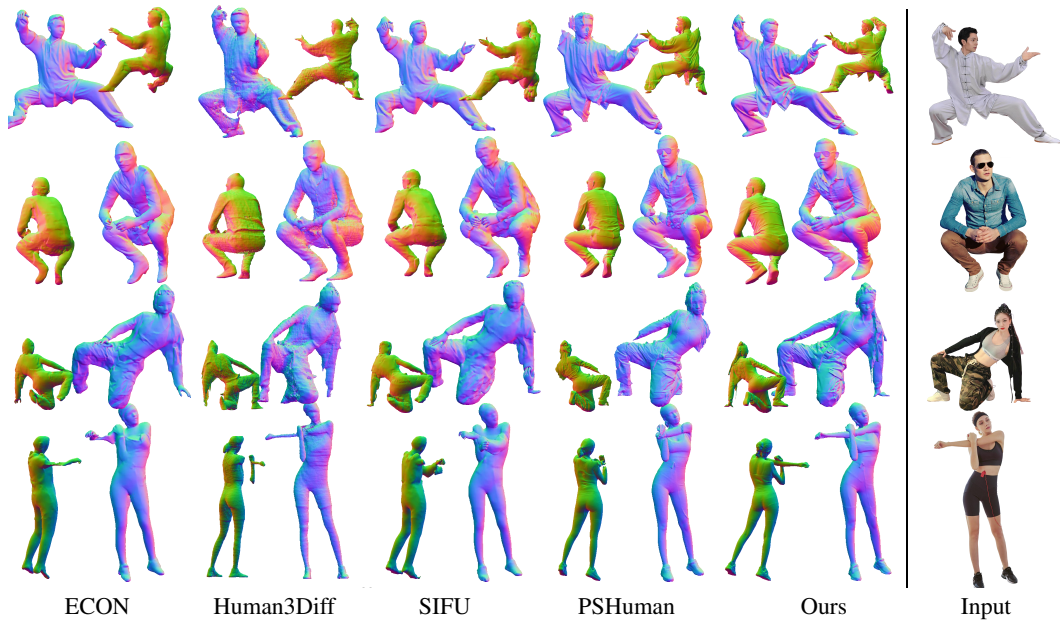


Figure 5: Geometry comparisons between ECON [81], Human3Diff [66], SIFU [78], PSHuman [25] and ours. Our method could reconstruct 3D shapes with complete body structure and rich details.



Figure 6: Appearance qualitative comparisons between GTA [81], Human3Diff [66], SIFU [78], PSHuman [25] and our method.

Table 1: Quantitative comparison of geometry and appearance on the CAPE-NFP [32], CAPE-FP [32], X-Humans [32] datasets. Our method achieves superior performance on all metrics than baseline methods.

| Method          | CAPE-NFP |        |        | CAPE-FP |        |        | X-Humans |        |        |         |        |        |
|-----------------|----------|--------|--------|---------|--------|--------|----------|--------|--------|---------|--------|--------|
|                 | Cham.↓   | P2S↓   | NC↑    | Cham.↓  | P2S↓   | NC↑    | Cham.↓   | P2S↓   | NC↑    | PSNR↑   | SSIM↑  | LPIPS↓ |
| ICON [63]       | 1.5966   | 1.4171 | 0.7974 | 1.2698  | 1.2018 | 0.8330 | 1.4971   | 1.3920 | 0.8133 | –       | –      | –      |
| ECON [62]       | 1.8335   | 1.5391 | 0.7731 | 1.3729  | 1.2962 | 0.8225 | 1.6425   | 1.4398 | 0.8054 | –       | –      | –      |
| GTA [77]        | 1.6311   | 1.5053 | 0.7890 | 1.2980  | 1.2457 | 0.8277 | 1.5050   | 1.4662 | 0.8044 | 20.0084 | 0.8502 | 0.1129 |
| SiFU [78]       | 1.6573   | 1.5130 | 0.7895 | 1.2759  | 1.2275 | 0.8289 | 1.5391   | 1.4331 | 0.8093 | 20.6747 | 0.8455 | 0.1104 |
| SiTH [13]       | 1.6461   | 1.2043 | 0.7914 | 1.0377  | 0.9767 | 0.8516 | 1.5104   | 1.4345 | 0.7972 | 19.8245 | 0.8204 | 0.1182 |
| Human3Diff [66] | 1.5991   | 1.2016 | 0.7427 | 0.9666  | 0.9340 | 0.7914 | 1.5034   | 1.4219 | 0.7468 | 19.7181 | 0.8065 | 0.1334 |
| PSHuman [25]    | 1.3726   | 0.9863 | 0.8276 | 0.7764  | 0.6527 | 0.8850 | 1.4377   | 1.1385 | 0.8393 | 20.8405 | 0.8523 | 0.0980 |
| TRELLIS [61]    | 2.0877   | 1.5678 | 0.7521 | 1.1155  | 1.0663 | 0.8353 | 2.0043   | 1.5053 | 0.7718 | 17.0786 | 0.7238 | 0.1529 |
| OURS            | 0.9127   | 0.8113 | 0.8483 | 0.6409  | 0.5962 | 0.8958 | 0.8353   | 0.7593 | 0.8872 | 21.8385 | 0.8741 | 0.0786 |

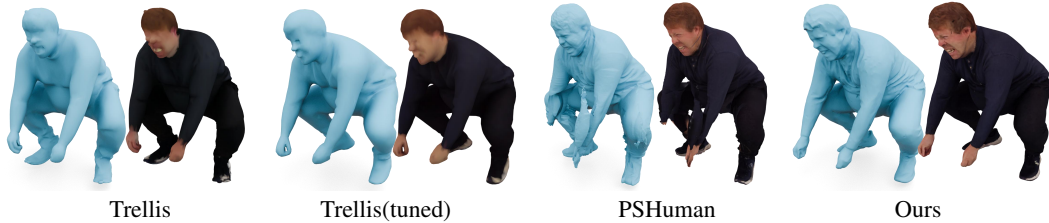


Figure 7: Ablation study of the 2D-3D synchronization attention for a joint 2D-3D modeling between PSHuman [25], fine-tuned Trellis [61], and our model.

## 4.2 Comparison with baseline methods

**Baselines.** We conducted a comprehensive comparison of our method against state-of-the-art single-view human reconstruction approaches, including classic implicit function based methods (ICON [63], GTA [77], SiFU [78]), explicit work (ECON [62]), and other baselines with generative priors (SiTH [13], Human3Diff [66] and PSHuman [25]). All evaluations are conducted with the official open-source codes, applying a unified evaluation method. More comparisons and visual results are provided in the Appendix.

**Comparison of geometry quality.** Combining the advantages of accurate 3D coarse structure from the native 3D generative model and the rich details of the multiview generative model, our method outperforms existing approaches in geometry quality as shown in Tab. 1. The qualitative comparison in Fig. 5 highlights that our method also handles complex human poses correctly, demonstrating significant improvements in structural integrity, correctness, and detail richness over baseline methods.

**Comparison of appearance quality.** We render four views with resolution of 768 for each sample and evaluate the appearance quality by reporting average PSNR, SSIM, and LPIPS. The results presented in Tab. 1 demonstrate that our method significantly outperforms existing approaches on all metrics. As illustrated by the qualitative results in Fig. 6, our method generates high-quality appearances on novel viewpoints, delivering natural and photorealistic reconstruction quality. In contrast, existing methods exhibit notable limitations in both unseen views and occluded regions, including blurred colors and artifacts.

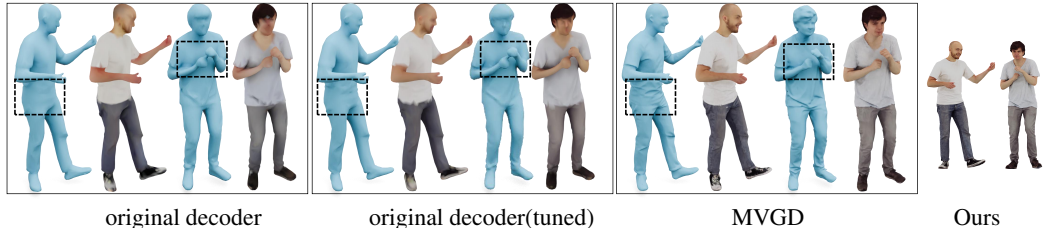


Figure 8: Ablation of different decoder settings. “original decoder” means the pretrained Trellis [61] decoder, while “original decoder (tuned)” and “multiview guided” are trained on the same human scans. All models use the same structured latents but decode them with different decoders.

Table 2: Ablation study of 2D-3D cross-space generative model on X-Humans [47] subset.

| Method               | PSNR $\uparrow$ | SSIM $\uparrow$ | LPIPS $\downarrow$ | Cham. Dist $\downarrow$ | P2S $\downarrow$ | NC $\uparrow$ |
|----------------------|-----------------|-----------------|--------------------|-------------------------|------------------|---------------|
| Trellis [61]         | 17.079          | 0.724           | 0.153              | 2.004                   | 1.505            | 0.772         |
| Trellis [61] (tuned) | 20.344          | 0.844           | 0.101              | 1.135                   | 1.041            | 0.848         |
| PSHuman [25]         | 20.840          | 0.852           | 0.098              | 1.438                   | 1.138            | 0.839         |
| Ours                 | <b>21.838</b>   | <b>0.874</b>    | <b>0.0786</b>      | <b>0.835</b>            | <b>0.759</b>     | <b>0.887</b>  |

Table 3: Ablation study of our multiview guided decoder (MVG D) on X-Humans [47] subset. All models employ the same structured latents but different decoders.

| Method                   | PSNR $\uparrow$ | SSIM $\uparrow$ | LPIPS $\downarrow$ | Cham. Dist $\downarrow$ | P2S $\downarrow$ | NC $\uparrow$ |
|--------------------------|-----------------|-----------------|--------------------|-------------------------|------------------|---------------|
| original decoder         | 21.083          | 0.862           | 0.092              | 0.895                   | 0.820            | 0.875         |
| original decoder (tuned) | 21.362          | 0.866           | 0.090              | 0.887                   | 0.810            | 0.877         |
| MVG D                    | <b>21.838</b>   | <b>0.874</b>    | <b>0.0786</b>      | <b>0.835</b>            | <b>0.759</b>     | <b>0.887</b>  |

### 4.3 Ablation Study

**2D-3D cross-space generative model.** We ablate the effectiveness of 2D-3D cross-space generative model on a X-Humans subset by removing the 2D-3D synchronization attention. For a fair comparison, we fine-tuned all the models on the same dataset. Compared with PSHuman (2D multiview generative model + remeshing) and Trellis (a native 3D generation model), this cross-space attention significantly enhances geometric accuracy and texture fidelity, as shown in Tab. 2 and Fig. 7.

**Multiview guided decoder (MVG D).** To evaluate the effect of MVGD, we compare three types of structured latent decoders: (1) the original Trellis decoder, (2) the Trellis decoder fine-tuned on human scans, and (3) the decoder guided with multiview images (our MVGD).

We conduct the comparison on the same X-Humans subset, evaluating both geometry and appearance. We apply mesh normalization and ICP registration to align the output meshes with the round truth scans to ensure a fair comparison. For each mesh, we render four views with a 768 resolution and report the average PSNR, SSIM, and LPIPS. The results in Tab. 3 show that multiview guided decoding significantly enhances geometric accuracy and texture quality. Fig. 8 also clearly illustrates that incorporating multiview image information improves the details and fidelity.

**Comparison between our structure and SMPL estimation.** To demonstrate that our structure handles some complex human poses better than the SMPL estimation, Fig. 9 shows the SMPL estimation from 4D-Humans [9] and the 3D structure generated by our method given the same input image. The SMPL estimation has obvious errors like self-intersection, while the structure generated by our method aligns better with the inputs without artifacts.

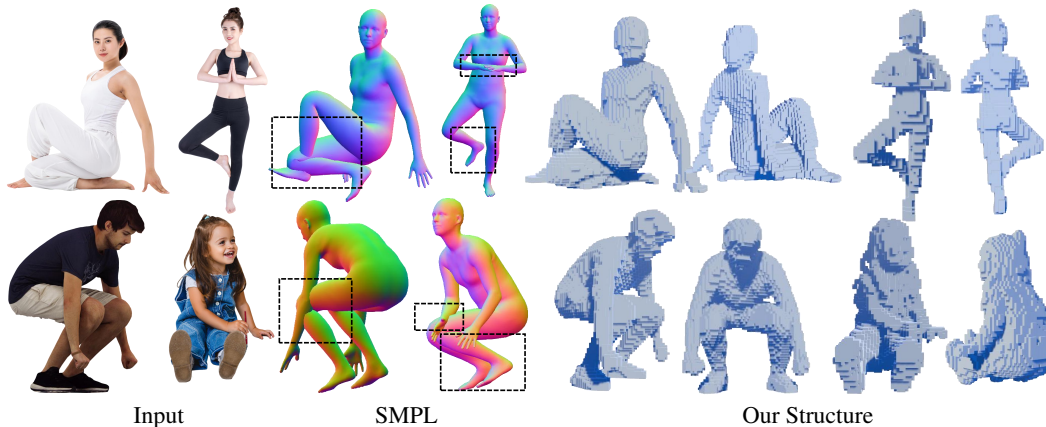


Figure 9: Robustness Analysis of the Generated Structure. The results demonstrate the robust reconstruction capabilities of our approach.

## 5 Limitation and Conclusion

In this work, we propose SyncHuman, a novel framework for robust 3D human generation from a single image. By introducing a 2D-3D cross-space generative model, we generate high-fidelity 3D structures and cross-view consistent multiview images. Then, we employ a multiview guided decoder to obtain detailed and structurally completed 3D human textured meshes. Extensive experiments demonstrate that SyncHuman can generate 3D humans with intricate geometric details and lifelike appearances, outperforming existing methods.



Figure 10: Unnatural textures under non-uniform lighting.

**Limitations.** Our method inherits certain constraints from the training data. First, since our training dataset is rendered with uniform light source, reconstructed textures may exhibit artifacts under extreme lighting conditions (e.g., localized overexposure or shadows, as shown in Fig. 10). Moreover, our multiview generation model is fine-tuned from SD 2.1 using only  $\sim 5,000$  human scans, so its generation quality is still constrained. It will be promising to scale up our model using video generative models or large-scale multiview human datasets in future work.

## References

- [1] Fabien Baradel\*, Matthieu Armando, Salma Galaoui, Romain Brégier, Philippe Weinzaepfel, Grégory Rogez, and Thomas Lucas\*. Multi-hmr: Multi-person whole-body human mesh recovery in a single shot. In *ECCV*, 2024.
- [2] Andreas Blattmann, Tim Dockhorn, Sumith Kulal, Daniel Mendelevitch, Maciej Kilian, Dominik Lorenz, Yam Levi, Zion English, Vikram Voleti, Adam Letts, et al. Stable video diffusion: Scaling latent video diffusion models to large datasets. *arXiv preprint arXiv:2311.15127*, 2023.
- [3] Zhongang Cai, Wanqi Yin, Ailing Zeng, Chen Wei, Qingping Sun, Wang Yanjun, Hui En Pang, Haiyi Mei, Mingyuan Zhang, Lei Zhang, et al. Smler-x: Scaling up expressive human pose and shape estimation. *Advances in Neural Information Processing Systems*, 36:11454–11468, 2023.
- [4] Jinnan Chen, Chen Li, Jianfeng Zhang, Lingting Zhu, Buzhen Huang, Hanlin Chen, and Gim Hee Lee. Generalizable human gaussians from single-view image. *arXiv preprint arXiv:2406.06050*, 2024.
- [5] Rui Chen, Jianfeng Zhang, Yixun Liang, Guan Luo, Weiyu Li, Jiarui Liu, Xiu Li, Xiaoxiao Long, Jiashi Feng, and Ping Tan. Dora: Sampling and benchmarking for 3d shape variational auto-encoders. *arXiv preprint arXiv:2412.17808*, 2024.
- [6] Julian Chibane, Thiemo Alldieck, and Gerard Pons-Moll. Implicit functions in feature space for 3d shape reconstruction and completion. In *Proceedings of the IEEE/CVF conference on computer vision and pattern recognition*, pages 6970–6981, 2020.
- [7] Yao Feng, Vasileios Choutas, Timo Bolkart, Dimitrios Tzionas, and Michael J. Black. Collaborative regression of expressive bodies using moderation. In *International Conference on 3D Vision (3DV)*, 2021.
- [8] Valentin Gabeur, Jean-Sebastien Franco, Xavier Martin, Cordelia Schmid, and Gregory Rogez. Moulding humans: Non-parametric 3d human shape estimation from single images. In *Proceedings of the IEEE/CVF International Conference on Computer Vision (ICCV)*, October 2019.
- [9] Shubham Goel, Georgios Pavlakos, Jathushan Rajasegaran, Angjoo Kanazawa, and Jitendra Malik. Humans in 4d: Reconstructing and tracking humans with transformers. In *Proceedings of the IEEE/CVF International Conference on Computer Vision*, pages 14783–14794, 2023.
- [10] Sang-Hun Han, Min-Gyu Park, Ju Hong Yoon, Ju-Mi Kang, Young-Jae Park, and Hae-Gon Jeon. High-fidelity 3d human digitization from single 2k resolution images. In *Proceedings of the IEEE/CVF Conference on Computer Vision and Pattern Recognition (CVPR)*, pages 12869–12879, June 2023.
- [11] Tong He, John Collomosse, Hailin Jin, and Stefano Soatto. Geo-pifu: Geometry and pixel aligned implicit functions for single-view human reconstruction. *Advances in Neural Information Processing Systems*, 33:9276–9287, 2020.

- [12] Hsuan-I Ho, Lixin Xue, Jie Song, and Otmar Hilliges. Learning locally editable virtual humans. In Proceedings of the IEEE/CVF Conference on Computer Vision and Pattern Recognition (CVPR), pages 21024–21035, June 2023.
- [13] I Ho, Jie Song, Otmar Hilliges, et al. Sith: Single-view textured human reconstruction with image-conditioned diffusion. In Proceedings of the IEEE/CVF Conference on Computer Vision and Pattern Recognition, pages 538–549, 2024.
- [14] Jonathan Ho and Tim Salimans. Classifier-free diffusion guidance. arXiv preprint arXiv:2207.12598, 2022.
- [15] Xin Huang, Ruizhi Shao, Qi Zhang, Hongwen Zhang, Ying Feng, Yebin Liu, and Qing Wang. Humannorm: Learning normal diffusion model for high-quality and realistic 3d human generation. In Proceedings of the IEEE/CVF Conference on Computer Vision and Pattern Recognition, pages 4568–4577, 2024.
- [16] Yangyi Huang, Hongwei Yi, Yuliang Xiu, Tingting Liao, Jiayang Tang, Deng Cai, and Justus Thies. Tech: Text-guided reconstruction of lifelike clothed humans. In 2024 International Conference on 3D Vision (3DV), pages 1531–1542. IEEE, 2024.
- [17] Zehuan Huang, Yuan-Chen Guo, Haoran Wang, Ran Yi, Lizhuang Ma, Yan-Pei Cao, and Lu Sheng. Mv-adapter: Multi-view consistent image generation made easy. arXiv preprint arXiv:2412.03632, 2024.
- [18] Yash Kant, Ethan Weber, Jin Kyu Kim, Rawal Khirodkar, Su Zhaoen, Julieta Martinez, Igor Gilitschenski, Shunsuke Saito, and Timur Bagautdinov. Pippo: High-resolution multi-view humans from a single image. arXiv preprint arXiv:2502.07785, 2025.
- [19] Bernhard Kerbl, Georgios Kopanas, Thomas Leimkühler, and George Drettakis. 3d gaussian splatting for real-time radiance field rendering. ToG, 42(4):1–14, 2023.
- [20] Byungjun Kim, Patrick Kwon, Kwangho Lee, Myunggi Lee, Sookwan Han, Daesik Kim, and Hanbyul Joo. Chupa: Carving 3d clothed humans from skinned shape priors using 2d diffusion probabilistic models. In Proceedings of the IEEE/CVF International Conference on Computer Vision (ICCV), pages 15965–15976, October 2023.
- [21] Samuli Laine, Janne Hellsten, Tero Karras, Yeongho Seol, Jaakko Lehtinen, and Timo Aila. Modular primitives for high-performance differentiable rendering. ACM Transactions on Graphics (ToG), 39(6):1–14, 2020.
- [22] Jiahao Li, Hao Tan, Kai Zhang, Zexiang Xu, Fajun Luan, Yinghao Xu, Yicong Hong, Kalyan Sunkavalli, Greg Shakhnarovich, and Sai Bi. Instant3d: Fast text-to-3d with sparse-view generation and large reconstruction model. arXiv preprint arXiv:2311.06214, 2023.
- [23] Mengfei Li, Xiaoxiao Long, Yixun Liang, Weiyu Li, Yuan Liu, Peng Li, Xiaowei Chi, Xingqun Qi, Wei Xue, Wenhan Luo, et al. M-Irm: Multi-view large reconstruction model. arXiv preprint arXiv:2406.07648, 2024.
- [24] Peng Li, Yuan Liu, Xiaoxiao Long, Feihu Zhang, Cheng Lin, Mengfei Li, Xingqun Qi, Shanghang Zhang, Wenhan Luo, Ping Tan, et al. Era3d: High-resolution multiview diffusion using efficient row-wise attention. arXiv preprint arXiv:2405.11616, 2024.
- [25] Peng Li, Wangguandong Zheng, Yuan Liu, Tao Yu, Yangguang Li, Xingqun Qi, Mengfei Li, Xiaowei Chi, Siyu Xia, Wei Xue, et al. Pshuman: Photorealistic single-view human reconstruction using cross-scale diffusion. arXiv preprint arXiv:2409.10141, 2024.
- [26] Weiyu Li, Jiarui Liu, Rui Chen, Yixun Liang, Xuelin Chen, Ping Tan, and Xiaoxiao Long. Craftsman: High-fidelity mesh generation with 3d native generation and interactive geometry refiner. arXiv preprint arXiv:2405.14979, 2024.
- [27] Yangguang Li, Zi-Xin Zou, Zexiang Liu, Dehu Wang, Yuan Liang, Zhipeng Yu, Xingchao Liu, Yuan-Chen Guo, Ding Liang, Wanli Ouyang, et al. Triposg: High-fidelity 3d shape synthesis using large-scale rectified flow models. arXiv preprint arXiv:2502.06608, 2025.
- [28] Tingting Liao, Hongwei Yi, Yuliang Xiu, Jiayang Tang, Yangyi Huang, Justus Thies, and Michael J Black. Tada! text to animatable digital avatars. arXiv preprint arXiv:2308.10899, 2023.
- [29] Yaron Lipman, Ricky TQ Chen, Heli Ben-Hamu, Maximilian Nickel, and Matt Le. Flow matching for generative modeling. arXiv preprint arXiv:2210.02747, 2022.

- [30] Yuan Liu, Cheng Lin, Zijiao Zeng, Xiaoxiao Long, Lingjie Liu, Taku Komura, and Wenping Wang. Syncdreamer: Generating multiview-consistent images from a single-view image. [arXiv preprint arXiv:2309.03453](#), 2023.
- [31] Xiaoxiao Long, Yuan-Chen Guo, Cheng Lin, Yuan Liu, Zhiyang Dou, Lingjie Liu, Yuexin Ma, Song-Hai Zhang, Marc Habermann, Christian Theobalt, and Wenping Wang. Wonder3d: Single image to 3d using cross-domain diffusion. In [Proceedings of the IEEE/CVF Conference on Computer Vision and Pattern Recognition \(CVPR\)](#), pages 9970–9980, June 2024.
- [32] Qianli Ma, Jinlong Yang, Anurag Ranjan, Sergi Pujades, Gerard Pons-Moll, Siyu Tang, and Michael J. Black. Learning to dress 3d people in generative clothing. In [Proceedings of the IEEE/CVF Conference on Computer Vision and Pattern Recognition \(CVPR\)](#), June 2020.
- [33] Shugao Ma, Tomas Simon, Jason Saragih, Dawei Wang, Yuecheng Li, Fernando De La Torre, and Yaser Sheikh. Pixel codec avatars. In [Proceedings of the IEEE/CVF Conference on Computer Vision and Pattern Recognition](#), pages 64–73, 2021.
- [34] Ryota Natsume, Shunsuke Saito, Zeng Huang, Weikai Chen, Chongyang Ma, Hao Li, and Shigeo Morishima. Siclope: Silhouette-based clothed people. In [Proceedings of the IEEE/CVF Conference on Computer Vision and Pattern Recognition \(CVPR\)](#), June 2019.
- [35] Maxime Oquab, Timothée Darcet, Théo Moutakanni, Huy Vo, Marc Szafraniec, Vasil Khalidov, Pierre Fernandez, Daniel Haziza, Francisco Massa, Alaaeldin El-Nouby, et al. Dinov2: Learning robust visual features without supervision. [arXiv preprint arXiv:2304.07193](#), 2023.
- [36] Sergio Orts-Escolano, Christoph Rhemann, Sean Fanello, Wayne Chang, Adarsh Kowdle, Yury Degtyarev, David Kim, Philip L Davidson, Sameh Khamis, Mingsong Dou, et al. Holoportation: Virtual 3d teleportation in real-time. In [Proceedings of the 29th annual symposium on user interface software and technology](#), pages 741–754, 2016.
- [37] Werner Palfinger. Continuous remeshing for inverse rendering. [Computer Animation and Virtual Worlds](#), 33(5):e2101, 2022.
- [38] Jeong Joon Park, Peter Florence, Julian Straub, Richard Newcombe, and Steven Lovegrove. DeepSDF: Learning continuous signed distance functions for shape representation. In [Proceedings of the IEEE/CVF Conference on Computer Vision and Pattern Recognition \(CVPR\)](#), June 2019.
- [39] Priyanka Patel and Michael J Black. Camerahr: Aligning people with perspective. [arXiv preprint arXiv:2411.08128](#), 2024.
- [40] William Peebles and Saining Xie. Scalable diffusion models with transformers. In [Proceedings of the IEEE/CVF international conference on computer vision](#), pages 4195–4205, 2023.
- [41] Lingteng Qiu, Xiaodong Gu, Peihao Li, Qi Zuo, Weichao Shen, Junfei Zhang, Kejie Qiu, Weihao Yuan, Guanying Chen, Zilong Dong, et al. Lhm: Large animatable human reconstruction model from a single image in seconds. [arXiv preprint arXiv:2503.10625](#), 2025.
- [42] Lingteng Qiu, Shenhao Zhu, Qi Zuo, Xiaodong Gu, Yuan Dong, Junfei Zhang, Chao Xu, Zhe Li, Weihao Yuan, Liefeng Bo, et al. Anigs: Animatable gaussian avatar from a single image with inconsistent gaussian reconstruction. In [Proceedings of the Computer Vision and Pattern Recognition Conference](#), pages 21148–21158, 2025.
- [43] Robin Rombach, Andreas Blattmann, Dominik Lorenz, Patrick Esser, and Björn Ommer. High-resolution image synthesis with latent diffusion models. In [CVPR](#), pages 10684–10695, 2022.
- [44] Robin Rombach, Andreas Blattmann, Dominik Lorenz, Patrick Esser, and Björn Ommer. High-resolution image synthesis with latent diffusion models. In [Proceedings of the IEEE/CVF Conference on Computer Vision and Pattern Recognition \(CVPR\)](#), pages 10684–10695, June 2022.
- [45] Shunsuke Saito, Zeng Huang, Ryota Natsume, Shigeo Morishima, Angjoo Kanazawa, and Hao Li. Pifu: Pixel-aligned implicit function for high-resolution clothed human digitization. In [Proceedings of the IEEE/CVF international conference on computer vision](#), pages 2304–2314, 2019.
- [46] Shunsuke Saito, Tomas Simon, Jason Saragih, and Hanbyul Joo. Pifuhd: Multi-level pixel-aligned implicit function for high-resolution 3d human digitization. In [Proceedings of the IEEE/CVF conference on computer vision and pattern recognition](#), pages 84–93, 2020.

- [47] Kaiyue Shen, Chen Guo, Manuel Kaufmann, Juan Jose Zarate, Julien Valentin, Jie Song, and Otmar Hilliges. X-avatar: Expressive human avatars. In Proceedings of the IEEE/CVF Conference on Computer Vision and Pattern Recognition, pages 16911–16921, 2023.
- [48] Tianchang Shen, Jacob Munkberg, Jon Hasselgren, Kangxue Yin, Zian Wang, Wenzheng Chen, Zan Gojcic, Sanja Fidler, Nicholas Sharp, and Jun Gao. Flexible isosurface extraction for gradient-based mesh optimization. ACM Transactions on Graphics (TOG), 42(4):1–16, 2023.
- [49] Yichun Shi, Peng Wang, Jianglong Ye, Mai Long, Kejie Li, and Xiao Yang. Mvdream: Multi-view diffusion for 3d generation. arXiv preprint arXiv:2308.16512, 2023.
- [50] David Smith, Matthew Loper, Xiaochen Hu, Paris Mavroidis, and Javier Romero. Facsimile: Fast and accurate scans from an image in less than a second. In Proceedings of the IEEE/CVF International Conference on Computer Vision (ICCV), October 2019.
- [51] Zhaoqi Su, Tao Yu, Yangang Wang, and Yebin Liu. Deepcloth: Neural garment representation for shape and style editing. IEEE Transactions on Pattern Analysis and Machine Intelligence, 45(2):1581–1593, 2022.
- [52] Jiaxiang Tang, Zhaoxi Chen, Xiaokang Chen, Tengfei Wang, Gang Zeng, and Ziwei Liu. Lgm: Large multi-view gaussian model for high-resolution 3d content creation. In European Conference on Computer Vision, pages 1–18. Springer, 2024.
- [53] Shitao Tang, Jiacheng Chen, Dilin Wang, Chengzhou Tang, Fuyang Zhang, Yuchen Fan, Vikas Chandra, Yasutaka Furukawa, and Rakesh Ranjan. Mvdiffusion++: A dense high-resolution multi-view diffusion model for single or sparse-view 3d object reconstruction. In European Conference on Computer Vision, pages 175–191. Springer, 2024.
- [54] Alexander Toshev and Christian Szegedy. Deeppose: Human pose estimation via deep neural networks. In Proceedings of the IEEE conference on computer vision and pattern recognition, pages 1653–1660, 2014.
- [55] Gul Varol, Duygu Ceylan, Bryan Russell, Jimei Yang, Ersin Yumer, Ivan Laptev, and Cordelia Schmid. Bodynet: Volumetric inference of 3d human body shapes. In Proceedings of the European Conference on Computer Vision (ECCV), September 2018.
- [56] Vikram Voleti, Chun-Han Yao, Mark Boss, Adam Letts, David Pankratz, Dmitry Tochilkin, Christian Laforde, Robin Rombach, and Varun Jampani. Sv3d: Novel multi-view synthesis and 3d generation from a single image using latent video diffusion. arXiv preprint arXiv:2403.12008, 2024.
- [57] Zhengyi Wang, Yikai Wang, Yifei Chen, Chendong Xiang, Shuo Chen, Dajiang Yu, Chongxuan Li, Hang Su, and Jun Zhu. Crm: Single image to 3d textured mesh with convolutional reconstruction model. In European Conference on Computer Vision, pages 57–74. Springer, 2024.
- [58] Zhou Wang, Alan C. Bovik, Hamid R. Sheikh, and Eero P. Simoncelli. Image quality assessment: from error visibility to structural similarity. IEEE Trans. Image Process., 13(4):600–612, 2004.
- [59] Kailu Wu, Fangfu Liu, Zhihan Cai, Runjie Yan, Hanyang Wang, Yating Hu, Yueqi Duan, and Kaisheng Ma. Unique3d: High-quality and efficient 3d mesh generation from a single image. In The Thirty-eighth Annual Conference on Neural Information Processing Systems, 2024.
- [60] Shuang Wu, Youtian Lin, Feihu Zhang, Yifei Zeng, Jingxi Xu, Philip Torr, Xun Cao, and Yao Yao. Direct3d: Scalable image-to-3d generation via 3d latent diffusion transformer. arXiv preprint arXiv:2405.14832, 2024.
- [61] Jianfeng Xiang, Zelong Lv, Sicheng Xu, Yu Deng, Ruicheng Wang, Bowen Zhang, Dong Chen, Xin Tong, and Jiaolong Yang. Structured 3d latents for scalable and versatile 3d generation. arXiv preprint arXiv:2412.01506, 2024.
- [62] Yuliang Xiu, Jinlong Yang, Xu Cao, Dimitrios Tzionas, and Michael J Black. Econ: Explicit clothed humans optimized via normal integration. In Proceedings of the IEEE/CVF conference on computer vision and pattern recognition, pages 512–523, 2023.
- [63] Yuliang Xiu, Jinlong Yang, Dimitrios Tzionas, and Michael J Black. Icon: Implicit clothed humans obtained from normals. In 2022 IEEE/CVF Conference on Computer Vision and Pattern Recognition (CVPR), pages 13286–13296. IEEE, 2022.
- [64] Jiale Xu, Weihao Cheng, Yiming Gao, Xintao Wang, Shenghua Gao, and Ying Shan. Instantmesh: Efficient 3d mesh generation from a single image with sparse-view large reconstruction models. arXiv preprint arXiv:2404.07191, 2024.

- [65] Yinghao Xu, Zifan Shi, Wang Yifan, Hansheng Chen, Ceyuan Yang, Sida Peng, Yujun Shen, and Gordon Wetzstein. Grm: Large gaussian reconstruction model for efficient 3d reconstruction and generation. In European Conference on Computer Vision, pages 1–20. Springer, 2024.
- [66] Yuxuan Xue, Xianghui Xie, Riccardo Marin, and Gerard Pons-Moll. Human 3diffusion: Realistic avatar creation via explicit 3d consistent diffusion models. arXiv preprint arXiv:2406.08475, 2024.
- [67] Xueting Yang, Yihao Luo, Yuliang Xiu, Wei Wang, Hao Xu, and Zhaoxin Fan. D-if: Uncertainty-aware human digitization via implicit distribution field. In Proceedings of the IEEE/CVF International Conference on Computer Vision (ICCV), pages 9122–9132, October 2023.
- [68] Yifan Yang, Dong Liu, Shuhai Zhang, Zeshuai Deng, Zixiong Huang, and Mingkui Tan. Hilo: Detailed and robust 3d clothed human reconstruction with high-and low-frequency information of parametric models. In Proceedings of the IEEE/CVF Conference on Computer Vision and Pattern Recognition, pages 10671–10681, 2024.
- [69] Yuhang Yang, Fengqi Liu, Yixing Lu, Qin Zhao, Pingyu Wu, Wei Zhai, Ran Yi, Yang Cao, Lizhuang Ma, Zheng-Jun Zha, et al. Sigman: Scaling 3d human gaussian generation with millions of assets. arXiv preprint arXiv:2504.06982, 2025.
- [70] Tao Yu, Zerong Zheng, Kaiwen Guo, Pengpeng Liu, Qionghai Dai, and Yebin Liu. Function4d: Real-time human volumetric capture from very sparse consumer rgbd sensors. In Proceedings of the IEEE/CVF Conference on Computer Vision and Pattern Recognition (CVPR), pages 5746–5756, June 2021.
- [71] Biao Zhang, Jiapeng Tang, Matthias Niessner, and Peter Wonka. 3dshape2vecset: A 3d shape representation for neural fields and generative diffusion models. arXiv preprint arXiv:2301.11445, 2023.
- [72] Hongwen Zhang, Yating Tian, Yuxiang Zhang, Mengcheng Li, Liang An, Zhenan Sun, and Yebin Liu. Pymaf-x: Towards well-aligned full-body model regression from monocular images. IEEE Transactions on Pattern Analysis and Machine Intelligence, 45(10):12287–12303, 2023.
- [73] Longwen Zhang, Ziyu Wang, Qixuan Zhang, Qiwei Qiu, Anqi Pang, Haoran Jiang, Wei Yang, Lan Xu, and Jingyi Yu. Clay: A controllable large-scale generative model for creating high-quality 3d assets. ACM Transactions on Graphics (TOG), 43(4):1–20, 2024.
- [74] Lvmin Zhang, Anyi Rao, and Maneesh Agrawala. Adding conditional control to text-to-image diffusion models. In Proceedings of the IEEE/CVF international conference on computer vision, pages 3836–3847, 2023.
- [75] Richard Zhang, Phillip Isola, Alexei A. Efros, Eli Shechtman, and Oliver Wang. The unreasonable effectiveness of deep features as a perceptual metric. In CVPR, pages 586–595. Computer Vision Foundation / IEEE Computer Society, 2018.
- [76] Richard Zhang, Phillip Isola, Alexei A. Efros, Eli Shechtman, and Oliver Wang. The unreasonable effectiveness of deep features as a perceptual metric. In CVPR, pages 586–595. Computer Vision Foundation / IEEE Computer Society, 2018.
- [77] Zechuan Zhang, Li Sun, Zongxin Yang, Ling Chen, and Yi Yang. Global-correlated 3d-decoupling transformer for clothed avatar reconstruction. Advances in Neural Information Processing Systems, 36, 2024.
- [78] Zechuan Zhang, Zongxin Yang, and Yi Yang. Sifu: Side-view conditioned implicit function for real-world usable clothed human reconstruction. In Proceedings of the IEEE/CVF Conference on Computer Vision and Pattern Recognition, pages 9936–9947, 2024.
- [79] Zibo Zhao, Zeqiang Lai, Qingxiang Lin, Yunfei Zhao, Haolin Liu, Shuhui Yang, Yifei Feng, Mingxin Yang, Sheng Zhang, Xianghui Yang, et al. Hunyuan3d 2.0: Scaling diffusion models for high resolution textured 3d assets generation. arXiv preprint arXiv:2501.12202, 2025.
- [80] Zibo Zhao, Wen Liu, Xin Chen, Xianfang Zeng, Rui Wang, Pei Cheng, Bin Fu, Tao Chen, Gang Yu, and Shenghua Gao. Michelangelo: Conditional 3d shape generation based on shape-image-text aligned latent representation. Advances in neural information processing systems, 36:73969–73982, 2023.
- [81] Ruichen Zheng, Peng Li, Haoqian Wang, and Tao Yu. Learning visibility field for detailed 3d human reconstruction and relighting. In Proceedings of the IEEE/CVF Conference on Computer Vision and Pattern Recognition (CVPR), pages 216–226, June 2023.

- [82] Zerong Zheng, Tao Yu, Yebin Liu, and Qionghai Dai. Pamir: Parametric model-conditioned implicit representation for image-based human reconstruction. IEEE transactions on pattern analysis and machine intelligence, 44(6):3170–3184, 2021.
- [83] Zerong Zheng, Tao Yu, Yixuan Wei, Qionghai Dai, and Yebin Liu. Deephuman: 3d human reconstruction from a single image. In Proceedings of the IEEE/CVF International Conference on Computer Vision (ICCV), October 2019.
- [84] Yiyu Zhuang, Jiayi Lv, Hao Wen, Qing Shuai, Ailing Zeng, Hao Zhu, Shifeng Chen, Yujiu Yang, Xun Cao, and Wei Liu. Idol: Instant photorealistic 3d human creation from a single image. arXiv preprint arXiv:2412.14963, 2024.
- [85] Qi Zuo, Xiaodong Gu, Lingteng Qiu, Yuan Dong, Weihao Yuan, Rui Peng, Siyu Zhu, Liefeng Bo, Zilong Dong, Qixing Huang, et al. Videomv: Consistent multi-view generation based on large video generative model. 2024.

## NeurIPS Paper Checklist

### 1. Claims

Question: Do the main claims made in the abstract and introduction accurately reflect the paper's contributions and scope?

Answer: [Yes]

Justification: The claims presented in the abstract and introduction accurately reflect the core contributions and scope of the paper. They are well-supported by experimental results, demonstrating both validity and credibility.

Guidelines:

- The answer NA means that the abstract and introduction do not include the claims made in the paper.
- The abstract and/or introduction should clearly state the claims made, including the contributions made in the paper and important assumptions and limitations. A No or NA answer to this question will not be perceived well by the reviewers.
- The claims made should match theoretical and experimental results, and reflect how much the results can be expected to generalize to other settings.
- It is fine to include aspirational goals as motivation as long as it is clear that these goals are not attained by the paper.

### 2. Limitations

Question: Does the paper discuss the limitations of the work performed by the authors?

Answer: [Yes]

Justification: Our method inherits certain constraints from the training data. First, since our training dataset is rendered with uniform light source, reconstructed textures may exhibit artifacts under extreme lighting conditions. Moreover, our multiview generation model is fine-tuned from SD 2.1 using only  $\sim 5,000$  human scans, so its generation quality is still constrained.

Guidelines:

- The answer NA means that the paper has no limitation while the answer No means that the paper has limitations, but those are not discussed in the paper.
- The authors are encouraged to create a separate "Limitations" section in their paper.
- The paper should point out any strong assumptions and how robust the results are to violations of these assumptions (e.g., independence assumptions, noiseless settings, model well-specification, asymptotic approximations only holding locally). The authors should reflect on how these assumptions might be violated in practice and what the implications would be.
- The authors should reflect on the scope of the claims made, e.g., if the approach was only tested on a few datasets or with a few runs. In general, empirical results often depend on implicit assumptions, which should be articulated.
- The authors should reflect on the factors that influence the performance of the approach. For example, a facial recognition algorithm may perform poorly when image resolution is low or images are taken in low lighting. Or a speech-to-text system might not be used reliably to provide closed captions for online lectures because it fails to handle technical jargon.
- The authors should discuss the computational efficiency of the proposed algorithms and how they scale with dataset size.
- If applicable, the authors should discuss possible limitations of their approach to address problems of privacy and fairness.
- While the authors might fear that complete honesty about limitations might be used by reviewers as grounds for rejection, a worse outcome might be that reviewers discover limitations that aren't acknowledged in the paper. The authors should use their best judgment and recognize that individual actions in favor of transparency play an important role in developing norms that preserve the integrity of the community. Reviewers will be specifically instructed to not penalize honesty concerning limitations.

### 3. Theory assumptions and proofs

Question: For each theoretical result, does the paper provide the full set of assumptions and a complete (and correct) proof?

Answer: [NA]

Justification: This work do not contain theoretical result.

Guidelines:

- The answer NA means that the paper does not include theoretical results.
- All the theorems, formulas, and proofs in the paper should be numbered and cross-referenced.
- All assumptions should be clearly stated or referenced in the statement of any theorems.
- The proofs can either appear in the main paper or the supplemental material, but if they appear in the supplemental material, the authors are encouraged to provide a short proof sketch to provide intuition.
- Inversely, any informal proof provided in the core of the paper should be complemented by formal proofs provided in appendix or supplemental material.
- Theorems and Lemmas that the proof relies upon should be properly referenced.

#### 4. Experimental result reproducibility

Question: Does the paper fully disclose all the information needed to reproduce the main experimental results of the paper to the extent that it affects the main claims and/or conclusions of the paper (regardless of whether the code and data are provided or not)?

Answer: [Yes]

Justification: We report the experiment details and we will release related codes.

Guidelines:

- The answer NA means that the paper does not include experiments.
- If the paper includes experiments, a No answer to this question will not be perceived well by the reviewers: Making the paper reproducible is important, regardless of whether the code and data are provided or not.
- If the contribution is a dataset and/or model, the authors should describe the steps taken to make their results reproducible or verifiable.
- Depending on the contribution, reproducibility can be accomplished in various ways. For example, if the contribution is a novel architecture, describing the architecture fully might suffice, or if the contribution is a specific model and empirical evaluation, it may be necessary to either make it possible for others to replicate the model with the same dataset, or provide access to the model. In general, releasing code and data is often one good way to accomplish this, but reproducibility can also be provided via detailed instructions for how to replicate the results, access to a hosted model (e.g., in the case of a large language model), releasing of a model checkpoint, or other means that are appropriate to the research performed.
- While NeurIPS does not require releasing code, the conference does require all submissions to provide some reasonable avenue for reproducibility, which may depend on the nature of the contribution. For example
  - (a) If the contribution is primarily a new algorithm, the paper should make it clear how to reproduce that algorithm.
  - (b) If the contribution is primarily a new model architecture, the paper should describe the architecture clearly and fully.
  - (c) If the contribution is a new model (e.g., a large language model), then there should either be a way to access this model for reproducing the results or a way to reproduce the model (e.g., with an open-source dataset or instructions for how to construct the dataset).
  - (d) We recognize that reproducibility may be tricky in some cases, in which case authors are welcome to describe the particular way they provide for reproducibility. In the case of closed-source models, it may be that access to the model is limited in some way (e.g., to registered users), but it should be possible for other researchers to have some path to reproducing or verifying the results.

#### 5. Open access to data and code

Question: Does the paper provide open access to the data and code, with sufficient instructions to faithfully reproduce the main experimental results, as described in supplemental material?

Answer: [No]

Justification: Our evaluation uses the public datasets. We do not provide code in Supplementary Material. But they will be made publicly available once they have been fully prepared.

Guidelines:

- The answer NA means that paper does not include experiments requiring code.
- Please see the NeurIPS code and data submission guidelines (<https://nips.cc/public/guides/CodeSubmissionPolicy>) for more details.
- While we encourage the release of code and data, we understand that this might not be possible, so “No” is an acceptable answer. Papers cannot be rejected simply for not including code, unless this is central to the contribution (e.g., for a new open-source benchmark).

- The instructions should contain the exact command and environment needed to run to reproduce the results. See the NeurIPS code and data submission guidelines (<https://nips.cc/public/guides/CodeSubmissionPolicy>) for more details.
- The authors should provide instructions on data access and preparation, including how to access the raw data, preprocessed data, intermediate data, and generated data, etc.
- The authors should provide scripts to reproduce all experimental results for the new proposed method and baselines. If only a subset of experiments are reproducible, they should state which ones are omitted from the script and why.
- At submission time, to preserve anonymity, the authors should release anonymized versions (if applicable).
- Providing as much information as possible in supplemental material (appended to the paper) is recommended, but including URLs to data and code is permitted.

#### 6. Experimental setting/details

Question: Does the paper specify all the training and test details (e.g., data splits, hyperparameters, how they were chosen, type of optimizer, etc.) necessary to understand the results?

Answer: [Yes]

Justification: We discuss the training and test details in the section on experiments and supplementary.

Guidelines:

- The answer NA means that the paper does not include experiments.
- The experimental setting should be presented in the core of the paper to a level of detail that is necessary to appreciate the results and make sense of them.
- The full details can be provided either with the code, in appendix, or as supplemental material.

#### 7. Experiment statistical significance

Question: Does the paper report error bars suitably and correctly defined or other appropriate information about the statistical significance of the experiments?

Answer: [Yes]

Justification: The reported quantitative evaluations are listed in Tab. 1, Tab. 2, and Tab. 3.

Guidelines:

- The answer NA means that the paper does not include experiments.
- The authors should answer "Yes" if the results are accompanied by error bars, confidence intervals, or statistical significance tests, at least for the experiments that support the main claims of the paper.
- The factors of variability that the error bars are capturing should be clearly stated (for example, train/test split, initialization, random drawing of some parameter, or overall run with given experimental conditions).
- The method for calculating the error bars should be explained (closed form formula, call to a library function, bootstrap, etc.)
- The assumptions made should be given (e.g., Normally distributed errors).
- It should be clear whether the error bar is the standard deviation or the standard error of the mean.
- It is OK to report 1-sigma error bars, but one should state it. The authors should preferably report a 2-sigma error bar than state that they have a 96% CI, if the hypothesis of Normality of errors is not verified.
- For asymmetric distributions, the authors should be careful not to show in tables or figures symmetric error bars that would yield results that are out of range (e.g. negative error rates).
- If error bars are reported in tables or plots, The authors should explain in the text how they were calculated and reference the corresponding figures or tables in the text.

#### 8. Experiments compute resources

Question: For each experiment, does the paper provide sufficient information on the computer resources (type of compute workers, memory, time of execution) needed to reproduce the experiments?

Answer: [Yes]

Justification: We train SyncHuman with 8 H800 GPUs.

Guidelines:

- The answer NA means that the paper does not include experiments.

- The paper should indicate the type of compute workers CPU or GPU, internal cluster, or cloud provider, including relevant memory and storage.
- The paper should provide the amount of compute required for each of the individual experimental runs as well as estimate the total compute.
- The paper should disclose whether the full research project required more compute than the experiments reported in the paper (e.g., preliminary or failed experiments that didn't make it into the paper).

#### 9. Code of ethics

Question: Does the research conducted in the paper conform, in every respect, with the NeurIPS Code of Ethics <https://neurips.cc/public/EthicsGuidelines>?

Answer: [Yes]

Justification: This work conforms with the NeurIPS Code of Ethics.

Guidelines:

- The answer NA means that the authors have not reviewed the NeurIPS Code of Ethics.
- If the authors answer No, they should explain the special circumstances that require a deviation from the Code of Ethics.
- The authors should make sure to preserve anonymity (e.g., if there is a special consideration due to laws or regulations in their jurisdiction).

#### 10. Broader impacts

Question: Does the paper discuss both potential positive societal impacts and negative societal impacts of the work performed?

Answer: [Yes]

Justification: The paper includes the Broader Impacts statement in subsection Ethics Statement in Supp.

Guidelines:

- The answer NA means that there is no societal impact of the work performed.
- If the authors answer NA or No, they should explain why their work has no societal impact or why the paper does not address societal impact.
- Examples of negative societal impacts include potential malicious or unintended uses (e.g., disinformation, generating fake profiles, surveillance), fairness considerations (e.g., deployment of technologies that could make decisions that unfairly impact specific groups), privacy considerations, and security considerations.
- The conference expects that many papers will be foundational research and not tied to particular applications, let alone deployments. However, if there is a direct path to any negative applications, the authors should point it out. For example, it is legitimate to point out that an improvement in the quality of generative models could be used to generate deepfakes for disinformation. On the other hand, it is not needed to point out that a generic algorithm for optimizing neural networks could enable people to train models that generate Deepfakes faster.
- The authors should consider possible harms that could arise when the technology is being used as intended and functioning correctly, harms that could arise when the technology is being used as intended but gives incorrect results, and harms following from (intentional or unintentional) misuse of the technology.
- If there are negative societal impacts, the authors could also discuss possible mitigation strategies (e.g., gated release of models, providing defenses in addition to attacks, mechanisms for monitoring misuse, mechanisms to monitor how a system learns from feedback over time, improving the efficiency and accessibility of ML).

#### 11. Safeguards

Question: Does the paper describe safeguards that have been put in place for responsible release of data or models that have a high risk for misuse (e.g., pretrained language models, image generators, or scraped datasets)?

Answer: [Yes]

Justification: To mitigate the risks associated with our technology, we are implementing the following safeguards: Implementing an email checking system that requires users to acknowledge and agree to user guidelines before accessing our model. Integrating pre-trained facial recognition and human body detection models to identify and flag potentially sensitive content. Incorporating safeguard strategies in Stable Diffusion to filter sensitive and harmful input images, including Content Filtering, NSFW (Not Safe For Work) Detection, Watermarking and Tracing. Our code and pre-trained model will be released under strict licenses (like Ethical Source License) that explicitly prohibit illegal or unethical use.

Guidelines:

- The answer NA means that the paper poses no such risks.
- Released models that have a high risk for misuse or dual-use should be released with necessary safeguards to allow for controlled use of the model, for example by requiring that users adhere to usage guidelines or restrictions to access the model or implementing safety filters.
- Datasets that have been scraped from the Internet could pose safety risks. The authors should describe how they avoided releasing unsafe images.
- We recognize that providing effective safeguards is challenging, and many papers do not require this, but we encourage authors to take this into account and make a best faith effort.

## 12. Licenses for existing assets

Question: Are the creators or original owners of assets (e.g., code, data, models), used in the paper, properly credited and are the license and terms of use explicitly mentioned and properly respected?

Answer: [Yes]

Justification: This paper cites the related datasets and codes used in our work.

Guidelines:

- The answer NA means that the paper does not use existing assets.
- The authors should cite the original paper that produced the code package or dataset.
- The authors should state which version of the asset is used and, if possible, include a URL.
- The name of the license (e.g., CC-BY 4.0) should be included for each asset.
- For scraped data from a particular source (e.g., website), the copyright and terms of service of that source should be provided.
- If assets are released, the license, copyright information, and terms of use in the package should be provided. For popular datasets, [paperswithcode.com/datasets](https://paperswithcode.com/datasets) has curated licenses for some datasets. Their licensing guide can help determine the license of a dataset.
- For existing datasets that are re-packaged, both the original license and the license of the derived asset (if it has changed) should be provided.
- If this information is not available online, the authors are encouraged to reach out to the asset's creators.

## 13. New assets

Question: Are new assets introduced in the paper well documented and is the documentation provided alongside the assets?

Answer: [NA]

Justification: The paper does not release new assets.

Guidelines:

- The answer NA means that the paper does not release new assets.
- Researchers should communicate the details of the dataset/code/model as part of their submissions via structured templates. This includes details about training, license, limitations, etc.
- The paper should discuss whether and how consent was obtained from people whose asset is used.
- At submission time, remember to anonymize your assets (if applicable). You can either create an anonymized URL or include an anonymized zip file.

## 14. Crowdsourcing and research with human subjects

Question: For crowdsourcing experiments and research with human subjects, does the paper include the full text of instructions given to participants and screenshots, if applicable, as well as details about compensation (if any)?

Answer: [NA]

Justification: Although the method involves 3D human models, we rely on datasets collected before this work; we refer to them for their specifics [1,2,3,4,5,6]. [1] Function4D: Real-time Human Volumetric Capture from Very Sparse RGBD Sensors [2] High-fidelity 3D Human Digitization from Single 2K Resolution Images [3] Learning Locally Editable Virtual Humans [4] DeepCloth: Neural Garment Representation for Shape and Style Editing [5] Learning to Dress 3D People in Generative Clothing [6] X-Avatar: Expressive Human Avatars

Guidelines:

- The answer NA means that the paper does not involve crowdsourcing nor research with human subjects.
- Including this information in the supplemental material is fine, but if the main contribution of the paper involves human subjects, then as much detail as possible should be included in the main paper.
- According to the NeurIPS Code of Ethics, workers involved in data collection, curation, or other labor should be paid at least the minimum wage in the country of the data collector.

15. **Institutional review board (IRB) approvals or equivalent for research with human subjects**

Question: Does the paper describe potential risks incurred by study participants, whether such risks were disclosed to the subjects, and whether Institutional Review Board (IRB) approvals (or an equivalent approval/review based on the requirements of your country or institution) were obtained?

Answer: [NA]

Justification: The paper does not involve crowdsourcing nor research with human subjects.

Guidelines:

- The answer NA means that the paper does not involve crowdsourcing nor research with human subjects.
- Depending on the country in which research is conducted, IRB approval (or equivalent) may be required for any human subjects research. If you obtained IRB approval, you should clearly state this in the paper.
- We recognize that the procedures for this may vary significantly between institutions and locations, and we expect authors to adhere to the NeurIPS Code of Ethics and the guidelines for their institution.
- For initial submissions, do not include any information that would break anonymity (if applicable), such as the institution conducting the review.

16. **Declaration of LLM usage**

Question: Does the paper describe the usage of LLMs if it is an important, original, or non-standard component of the core methods in this research? Note that if the LLM is used only for writing, editing, or formatting purposes and does not impact the core methodology, scientific rigorosity, or originality of the research, declaration is not required.

Answer: [NA]

Justification: Our method does not involve LLMs as any important, original, or non-standard components.

Guidelines:

- The answer NA means that the core method development in this research does not involve LLMs as any important, original, or non-standard components.
- Please refer to our LLM policy (<https://neurips.cc/Conferences/2025/LLM>) for what should or should not be described.

## A Details

### A.1 Training Details

**2D-3D Cross-Space Generative Model.** Our 2D-3D Cross-Space generative model was trained on 8 NVIDIA H800 GPUs. For the multiview generative model branch, we adopt the architecture of PSHuman [25] but retrain it using flow matching from the open-source pre-trained text-to-image generation model, SD2.1-unclip [43]. We train the multiview generation branch separately with a batch size of 32 for a total of 30,000 iterations. We adopt an adaptive learning rate schedule, initializing the learning rate at  $1e-4$  and decreasing it to  $5e-5$  after 2,000 steps. For 2D-3D Cross-Space generative model, we initialize the network weights using: the fine-tuned weights from our multiview generation branch (as described above), a pre-trained image-to-3D model (Trellis [61]). Additionally, we perform zero-initialization on the output layer of the 2D-3D synchronization attention module. We train the 2D-3D Cross-Space generative model with a batch size of 32 for a total of 50,000 iterations. We adopt an adaptive learning rate schedule, initializing the learning rate at  $2.5e-5$  and decreasing it to  $1.25e-5$  after 2,000 steps. To enable class-free guidance (CFG) [14] during inference, we randomly omit the image condition at a rate of 0.05 during training.

**Multiview Guided Decoder.** Our Multiview Guided Decoder was trained on 1 NVIDIA H800 GPU. We train the decoder with a batch size of 4 for a total of 14,000 iterations, using a learning rate of  $1e-4$ .

The loss design largely adheres to Trellis [61]’s setup. For the GS decoder, the loss includes reconstruction loss and regularization loss, with regularizations employed for the volume and opacity of the Gaussians to prevent their degeneration, specifically to avoid them becoming excessively large or transparent.  $\mathcal{L}_{\text{recon}}$  is composed of  $\mathcal{L}_1$  (L1 loss), Structural Similarity Index (SSIM), and Learned Perceptual Image Patch Similarity (LPIPS). The full training objective is defined as follows:

$$\mathcal{L}_{\text{GS}} = \mathcal{L}_{\text{recon}} + \mathcal{L}_{\text{vol}} + \mathcal{L}_{\alpha} \quad (5)$$

where:

$$\begin{aligned} \mathcal{L}_{\text{recon}} &= \mathcal{L}_1 + 0.2(1 - \text{SSIM}) + 0.2 \cdot \text{LPIPS}, \\ \mathcal{L}_{\text{vol}} &= \frac{1}{LK} \sum_{i=1}^L \sum_{k=1}^K \prod s_i^k, \\ \mathcal{L}_{\alpha} &= \frac{1}{LK} \sum_{i=1}^L \sum_{k=1}^K (1 - \alpha_i^k)^2, \end{aligned} \quad (6)$$

where  $L$  is the total number of active voxels. For each active voxel,  $K$  Gaussians are predicted,  $s$  and  $\alpha$  are the scale and opacity of Gaussian, respectively.

For the mesh decoder, we utilize Nvdiffrast [21] to render the extracted mesh along with its attributes, producing a foreground mask  $\mathbf{M}$ , a depth map  $\mathbf{D}$ , a normal map  $\mathbf{N}_m$  directly derived from the mesh, an RGB image  $\mathbf{C}$ , and a normal map  $\mathbf{N}$  from the predicted normals, a normal map  $\mathbf{N}_m^{\text{front}}$  directly derived from the mesh from the front view, an RGB image  $\mathbf{C}^{\text{front}}$  from the front view. The training objective is then defined as follows:

$$\mathcal{L}_{\text{M}} = \mathcal{L}_{\text{geo}} + 0.4\mathcal{L}_{\text{color}} + \mathcal{L}_{\text{reg}}, \quad (7)$$

where  $\mathcal{L}_{\text{geo}}$  and  $\mathcal{L}_{\text{color}}$  are written as:

$$\mathcal{L}_{\text{geo}} = \mathcal{L}_1(\mathbf{M}) + 10\mathcal{L}_{\text{Huber}}(\mathbf{D}) + \mathcal{L}_{\text{recon}}(\mathbf{N}_m) + 0.1\mathcal{L}_{\text{recon}}(\mathbf{N}_m^{\text{front}}) \quad (8)$$

$$\mathcal{L}_{\text{color}} = \mathcal{L}_{\text{recon}}(\mathbf{C}) + \mathcal{L}_{\text{recon}}(\mathbf{N}) + 0.1\mathcal{L}_{\text{recon}}(\mathbf{C}^{\text{front}}) \quad (9)$$

Here,  $\mathcal{L}_{\text{recon}}$  is defined identically to Eq. (7). Finally,  $\mathcal{L}_{\text{reg}}$  consists of three terms:

$$\mathcal{L}_{\text{reg}} = \mathcal{L}_{\text{consist}} + \mathcal{L}_{\text{dev}} + 0.01\mathcal{L}_{\text{tsdf}}, \quad (10)$$

where  $\mathcal{L}_{\text{consist}}$  penalizes the variance of attributes associated with the same voxel vertex,  $\mathcal{L}_{\text{dev}}$  is a regularization.

### A.2 Detailed Network Structure

**2D-3D synchronization attention.** In the 3D branch, we inserted two 2D-to-3D attention blocks after the 8th and 16th transformer blocks respectively. Similarly, for the 2D branch, we added two 3D-to-2D attention blocks following the 3rd CrossAttnDownBlockMV2D and the UpBlock2D modules.

**(1)2D-to-3D attention.** Each 3D voxel feature  $\mathbf{u}_i \in \mathbb{R}^{d_u}$  with coordinates  $(x_i, y_i, z_i)$  is orthographically projected onto four view normal map planes (front, back, left, right) to obtain corresponding 2D pixel features:

$$\mathbf{p}_i^v = \pi_v(\mathbf{u}_i), \quad v \in \text{front, back, left, right} \quad (11)$$

where  $\mathbf{p}_i^v \in \mathbb{R}^{d_p}$  is the projected 2D features, and  $\pi_v(\cdot)$  is the orthogonal projection function.

The 3D voxel feature  $\mathbf{u}_i$  and 2D pixel feature  $\mathbf{p}_i^v$  are respectively passed through the MLP transformation:

$$\mathbf{q}_i = \text{MLP}_q(\mathbf{u}_i) \quad \mathbf{k}_i^v = \text{MLP}_k(\mathbf{p}_i^v) \quad \mathbf{v}_i^v = \text{MLP}_v(\mathbf{p}_i^v) \quad (12)$$

Using 3D voxel feature as queries and concatenating four 2D pixel features along the sequence dimension as keys and values, compute the cross-attention:

$$\begin{aligned} \mathbf{K}_i &= \text{Concat} \left( \mathbf{k}_i^{\text{front}}, \mathbf{k}_i^{\text{back}}, \mathbf{k}_i^{\text{left}}, \mathbf{k}_i^{\text{right}} \right) \\ \mathbf{V}_i &= \text{Concat} \left( \mathbf{v}_i^{\text{front}}, \mathbf{v}_i^{\text{back}}, \mathbf{v}_i^{\text{left}}, \mathbf{v}_i^{\text{right}} \right) \\ \mathbf{u}'_i &= \mathbf{u}_i + \text{MLP} \left( \text{Softmax} \left( \frac{\mathbf{q}_i \mathbf{K}_i^T}{\sqrt{d}} \right) \mathbf{V}_i \right) \end{aligned} \quad (13)$$

Here,  $\mathbf{u}'_i$  represents the updated 3D voxel feature.

**(2)3D-to-2D attention.** Let the input consist of 2D pixel features  $\mathbf{p}_i \in \mathbb{R}^{d_p}$  from a color map or a normal map, with a corresponding 3D voxel space represented by  $\mathbf{U} \in \mathbb{R}^{X \times Y \times Z \times d_u}$ , where  $d_p$  and  $d_u$  denote the feature dimensions of 2D pixels and 3D voxels, respectively.

Each 2D pixel feature  $\mathbf{p}_i$  corresponds to a ray in a 3D space. Sampling  $H$  3D voxel features along this ray forms a 3D voxel feature sequence:

$$\mathcal{U}_i = \{\mathbf{u}_{i,j}\}_{j=1}^H, \quad \mathbf{u}_{i,j} \in \mathbb{R}^{d_u} \quad (14)$$

Where  $\mathbf{u}_{i,j}$  is the 3D voxel feature at the  $j$ -th depth position along the projection ray of 2D pixel feature  $\mathbf{p}_i$ .  $H$  is the length of the 3D voxel feature sequence.

The 2D pixel feature  $\mathbf{p}_i$  is mapped to a query vector, while each 3D voxel feature  $\mathbf{u}_{i,j}$  is mapped to a key and a value vector:

$$\mathbf{q}_i = \text{MLP}_q(\mathbf{p}_i) \quad \mathbf{k}_{i,j} = \text{MLP}_k(\mathbf{u}_{i,j}) \quad \mathbf{v}_{i,j} = \text{MLP}_v(\mathbf{u}_{i,j}) \quad (15)$$

By concatenating all key vectors and value vectors across the sequence of 3D voxel features, we construct the complete key and value matrices as:

$$\mathbf{K}_i = [\mathbf{k}_{i,1}, \mathbf{k}_{i,2}, \dots, \mathbf{k}_{i,H}] \in \mathbb{R}^{H \times d}, \quad \mathbf{V}_i = [\mathbf{v}_{i,1}, \mathbf{v}_{i,2}, \dots, \mathbf{v}_{i,H}] \in \mathbb{R}^{H \times d} \quad (16)$$

Compute the attention output with the 2D pixel feature  $\mathbf{q}_i$  as the query, and the 3D voxel feature  $\mathbf{K}_i$  and  $\mathbf{V}_i$  as the key and value:

$$\mathbf{p}'_i = \mathbf{p}_i + \text{MLP} \left( \text{Softmax} \left( \frac{\mathbf{q}_i \mathbf{K}_i^T}{\sqrt{d}} \right) \mathbf{V}_i \right) \quad (17)$$

Here,  $\mathbf{p}'_i$  represents the updated 2D pixel feature.

**Multiview Guided Decoder (MVG D).** The 3d sparse structure  $\mathcal{V}_{\text{grid}}$  is first processed by the Structured Latents generative model, which denoises it into a structured latent  $\mathbf{z}$ . For multiview color and normal images, we first upsample the images, then we extract multilevel local patch features using the DINOv2 backbone from layers  $l \in \{4, 11, 17, 23\}$  per image:

$$\mathbf{F}_i^{(l)} = \text{DINOv2}_l(\mathbf{I}_i^{\text{up}}) \in \mathbb{R}^{V \times V \times d}. \quad (18)$$

The features from different layers are concatenated and then processed through a MLP to form the final representation:

$$\mathbf{F}_i = \text{MLP}(\text{Concat}(\mathbf{F}_i^{(4)}, \mathbf{F}_i^{(11)}, \mathbf{F}_i^{(17)}, \mathbf{F}_i^{(23)})) \in \mathbb{R}^{V \times V \times d} \quad (19)$$

Given a voxel position  $\mathbf{p} = (x, y, z)$ , its projection onto the  $i$ -th view yields the corresponding pixel coordinates:

$$\pi_i(\mathbf{p}) = (u_i, v_i), \quad \text{where } u_i, v_i \in 0, 1, \dots, V - 1. \quad (20)$$

The corresponding image features are then retrieved via direct indexing:

$$\mathbf{f}_i(\mathbf{p}) = \mathbf{F}_i[u_i, v_i] \in \mathbb{R}^d. \quad (21)$$

The injection feature is constructed by concatenating the structured latent at position  $\mathbf{p}$  ( $\mathbf{z}_{\mathbf{p}} \in \mathbb{R}^{d_z}$ ) with multiview pixel-aligned features obtained from the color and normal maps of 4 views (8 feature vectors in total). Formally,

$$\mathbf{z}_{\text{inj}} = \text{Concat}(\mathbf{z}_{\mathbf{p}}, \mathbf{f}_1(\mathbf{p}), \dots, \mathbf{f}_8(\mathbf{p})) \in \mathbb{R}^{d_z + 8 \times d}. \quad (22)$$

This injection feature is then processed by an MLP to refine the structured latent representation:

$$\mathbf{z}'_{\mathbf{p}} = \mathbf{z}_{\mathbf{p}} + \text{MLP}(\mathbf{z}_{\text{inj}}) \in \mathbb{R}^{d_z}. \quad (23)$$

We insert a multiview injection module after each self-attention in the decoder. We apply the same multiview feature injection mechanism to both the mesh decoder and the GS decoder, resulting in refined mesh and GS representations.



Figure 11: Qualitative comparison of SyncHuman with Gaussians-based methods (LHM, IDOL) and a native 3D model (Hunyuan3D 2.5). SyncHuman achieves visually high-fidelity results.

## B More Experiment

### B.1 More Results

**Comparison with Gaussians-based Methods and Native 3D generative model.** To further evaluate the effectiveness of our method, we conduct a qualitative comparison between SyncHuman and two Gaussians-based methods (LHM [41] and IDOL [84]), as well as a more advanced native 3D model, Hunyuan3D 2.5 [79], as shown in Fig. 11. All these methods are capable of producing structurally plausible and visually reasonable results. Since LHM and IDOL are based on Gaussians, they can only produce RGB images through rendering. For comparison, we render RGB images from the front view. Both LHM and IDOL rely on SMPL, and when SMPL estimation is inaccurate or fails, the resulting structure is correspondingly erroneous. Furthermore, as illustrated in Fig. 11, IDOL and LHM still exhibit limited fidelity. Hunyuan3D 2.5, trained on a large-scale dataset, is a native 3D model that can also produce reasonable human structures with details. However, as observed in Fig. 11, Hunyuan3D 2.5 produces human meshes with less fidelity.

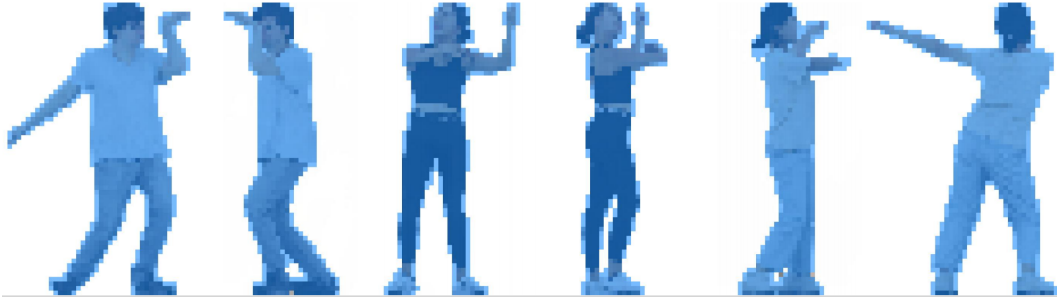


Figure 12: After alignment using 2D-3D attention, the multi-view projections of the two branches can almost completely overlap.

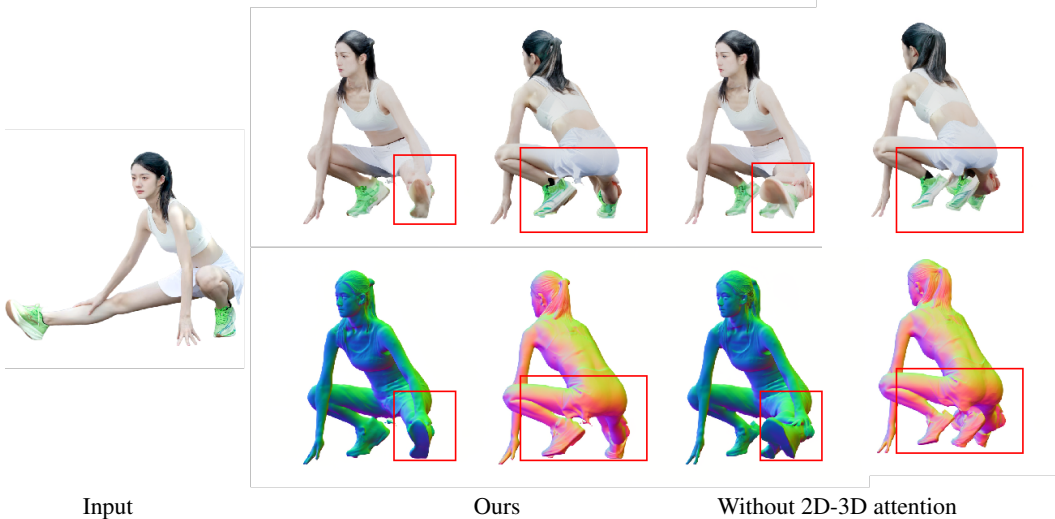


Figure 13: Comparison of the quality of intermediate multi-view generation with and without 2D-3D attention.

## B.2 Ablation of the quality of intermediate multi-view generation and 3D structure generation

We additionally report the quality of intermediate multi-view generation and 3D structure generation on a small human scan subset. IOU of the 3D structure generation: 0.5907 (with 2D-3D synchronization attention) vs. 0.4813 (without 2D-3D synchronization attention). Color and normal image quality improvements by 3D-2D attention:

Table 4: Comparison of different methods.

| Method           | PSNR $\uparrow$ | SSIM $\uparrow$ | LPIPS $\downarrow$ |
|------------------|-----------------|-----------------|--------------------|
| w/o att (color)  | 23.328          | 0.877           | 0.078              |
| ours (color)     | 24.027          | 0.894           | 0.070              |
| w/o att (normal) | 22.851          | 0.866           | 0.097              |
| ours (normal)    | 23.439          | 0.882           | 0.087              |

Because generating 3D structures or multiview images from single-view inputs has ambiguity, the generation results are not exactly the same as the ground-truth. However, our 2D-3D attention could produce results more similar to GT. This demonstrates that our 2D-3D synchronization attention could benefit both branches to improve the multiview generation quality and 3D structure quality. As in Fig. 12, after alignment using 2D-3D attention, the multi-view projections of the two branches can almost completely overlap. And as in Fig. 13, when with 2D-3D attention multiview images have a more reasonable human body structure.



Figure 14: Visualization of the unconditional generation task.

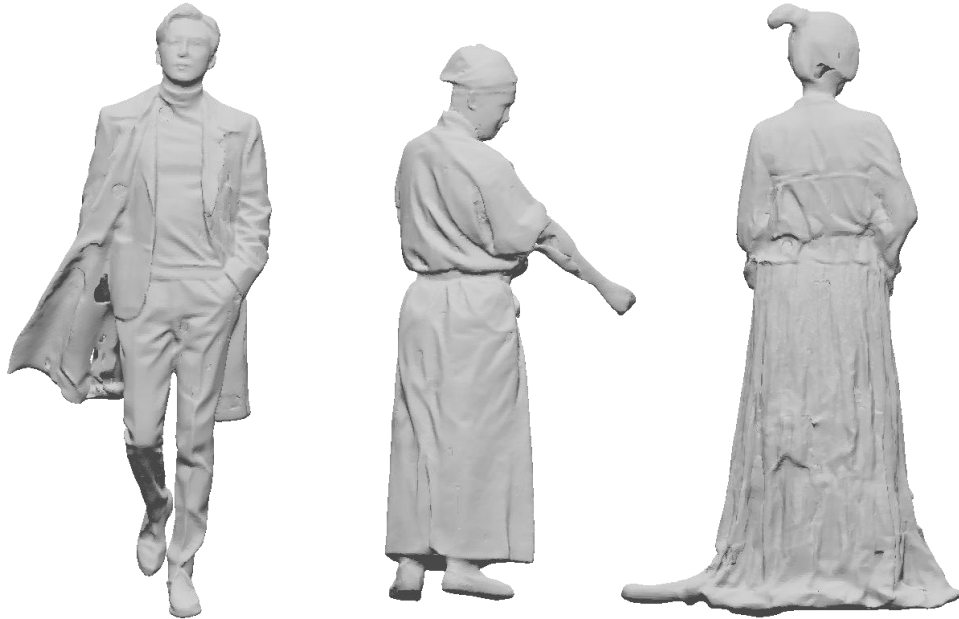


Figure 15: In some cases, the decoded mesh may contain some holes on the surface.

### B.3 Inference time.

On a single H800, the inference time is as follows: ours 38.57s vs Trellis 15.68s vs PSHuman 52.98s Our method is faster than PSHuman as it directly decodes a 3D shape without requiring additional differentiable rendering optimization. The slower speed compared to Trellis is due to our use of the 2D multi-view generation.

### B.4 Unconditional Generation.

We tested our model on the unconditional generation task as in Fig. 14. The generation quality is worse than the conditional generation from a single-view image.

## C discussion

### C.1 Limitations about containing holes in the generation

Our method is based on Trellis [61], which uses FlexiCube [48] in the trellis mesh decoder branch does not put a water-tight constraint on the surfaces. Thus, holes may appear on the surface in some cases, as shown in Fig. 15. A possible way to make the generated meshes water-tight is to adopt another SDF fitting on the generated mesh. Alternatively, we may adopt other 3D native generative models using SDFs as targets, like Hunyuan3D [79] or TripoSG [27], to avoid this problem. We leave this for future work.

## C.2 Differences from SyncDreamer.

Our method fundamentally differs from SyncDreamer in the following two aspects. First, the synchronization subjects are totally different. SyncDreamer synchronizes the generation of multiview 2D images, whereas our method synchronizes the 2D generative model and the 3D native generative model. Our method demonstrates that simultaneously generating multiview images and 3D representations benefits each other and greatly improves the 3D generation quality. We inject information in both directions, 2D to 3D and 3D to 2D. Second, the functionality and design of the volume in our method are fundamentally different from those in SyncDreamer. SyncDreamer constructs a feature volume to share information among different views. In contrast, in our method, the volume is a meaningful 3D representation generated from noise.

## C.3 Ethics Statement

The objective of SyncHuman is to equip users with a powerful tool for creating realistic clothed 3D human models. By enabling 3D human generation from a single image, our method supports diverse ethnicities and populations, promoting equitable cultural representation. Our model was trained on the public datasets THuman2.1 [70], CustomHumans [12], THuman3.0 [51], and 2K2K [10], and tested on X-Humans [47] and CAPE [32]. However, there is a potential risk that these generated models could be misused to deceive viewers (e.g., adult content, political manipulation, exploitation of artists via digital replicas.). It is noted that this issue is not unique to our methodology but prevalent in other human generative methodologies. Therefore, it is absolutely essential for current and future research in the field of 3D human generative modeling to address and reassess these considerations consistently.